# Simulation Study of a Positive Ionospheric Storm Phase Observed at Millstone Hill

M. Swisdak,[1] J. D. Huba,[2] G. Joyce[1], and Chao-Song Huang[3]

M. Swisdak, Icarus Research, Inc., PO Box 30780 Bethesda MD 20824-0780, USA , (swisdak@ppd.nrl.navy.mil)

[1]Icarus Research, Inc., Bethesda, MD, USA.

[2]Plasma Physics Division, Naval Research Laboratory, Washington, DC, USA.

[3]Haystack Observatory, Massachusetts Institute of Technology, Westford, Massachusetts

**Abstract.**

Simulation results from the NRL ionospheric model SAMI2 indicate that the changes in the F-region over Millstone Hill during the geomagnetic storm beginning on 3 April 2004 are primarily due to the influence of a long-lasting eastward electric field, as was previously suggested by *Huang et al.* [2005]. A simulation of the storm day agrees well with the observational data and shows that, compared with the ionosphere of the previous quiet day, the peak electron density in the F-region ($N_mF_2$) increased by a factor of $\approx$ 2, the altitude of the peak density ($h_mF_2$) rose by $\approx 80$ km, and the F-region electron temperature decreased by $\approx 1000$ K. Further simulations in which either the neutral atmosphere and winds or the electric field were replaced by their quiet day counterparts clearly suggest that the electric field played the dominant, although not exclusive, role in producing these effects.

## 1. Introduction

After an extended quiet period lasting from 29 March to 2 April 2004 a magnetic storm began at 1412 UT on 3 April and reached a minimum Dst of -149 nT at 0042 UT on the following day. *Huang et al.* [2005] reported that this event triggered large, long-lasting changes in the daytime ionosphere, including a strong positive ionospheric storm phase (i.e., a period in which the F-region electron density increased). Understanding long-duration mid-latitude positive storms such as this is of particular interest because they have significant effects on large regions of the ionosphere. *Buonsanto* [1999] noted that the generation of such events is one of the main unresolved problems in ionospheric research.

Two mechanisms have been proposed as drivers of such dayside storms: winds in the neutral atmosphere and electric fields (see Figure 1). In the former, heat inputs in the auroral regions are thought to cause global changes in the wind circulation pattern and thermospheric composition [*Rishbeth et al.*, 1985; *Fuller-Rowell et al.*, 1994], including the generation of equatorward neutral winds that lift the mid-latitude F-region [*Jakowski et al.*, 1990; *Bauske and Prölls*, 1997; *Lu et al.*, 2001]. (In Figure 1, $\mathbf{V_n} \cdot \mathbf{B} < 0$ and the collisionally-coupled plasma is driven up the field lines.) On the other hand, *Foster and Rich* [1998] reported direct observations of the uplift of the mid-latitude ionosphere by a prompt penetration eastward electric field (in Figure 1 the $\mathbf{E} \times \mathbf{B}$ drift is upward and poleward). These processes are not completely distinct since, for example, equatorward neutral winds can maintain a dynamo electric field.

*Huang et al.* [2005] suggested that the proximate cause for the 3 April storm was an enhanced eastward electric field that lifted the mid-latitude ionosphere for several hours. In this Letter we present simulations that support this conclusion, although the neutral winds do seem to play a minor, but important, role. We describe our computational model SAMI2 in section 2, present the simulation results in section 3, and discuss our conclusions in section 4.

## 2. Computational Model

SAMI2 is a two-dimensional, semi-implicit, Eulerian fluid model of the low to mid-latitude ionosphere at one geomagnetic longitude [*Huba et al.*, 2000]. Previous studies have shown that SAMI2 simulations of the F-region electron density are in good agreement with data from both satellites [*Huba et al.*, 2002] and the Millstone Hill observatory [*Huba et al.*, 2003].

In this study the simulation domain passes through a point 330 km above Millstone Hill (42.6° N, 288.5° E, invariant latitude 55°) and has north-south extrema at geographic latitudes of −68.7° and 45.2°. We place 201 gridpoints along each of 114 field lines with non-uniform spacing in both dimensions to achieve better resolution at low altitudes. Test runs in which the number of points in either dimension is doubled suggest our results have converged. The first and last gridpoints of each field line are at an altitude of 85 km and the apexes range between 150 and 14,000 km ($L$ values of 1.02 to 3.20).

We model the terrestrial magnetic field as an offset, tilted dipole for which the center as well as the geographic latitude and longitude of the magnetic north pole have been chosen to maximize agreement in the simulation domain with the International Geomagnetic

Reference Field. Parallel to the field, i.e., along a flux tube, we solve the fluid continuity and momentum equations for seven ion species (H$^+$, He$^+$, N$^+$, O$^+$, N$_2^+$, NO$^+$, and O$_2^+$) and the temperature equation for three (H$^+$, He$^+$, and O$^+$). The temperatures of the other four ions are taken to be equal to that of O$^+$. To model the electrons we assume that the charge density and parallel current density vanish, which then determines the electron density and velocity parallel to the field; the electron temperature equation is solved separately. The empirical models NRLMSISE-00 and HWM93 [*Picone et al.*, 2002; *Hedin et al.*, 1991] specify the composition and winds of the neutral atmosphere, respectively.

We assume that transport perpendicular to the magnetic field is solely due to $\mathbf{E} \times \mathbf{B}$ drifts. To find the electric field throughout the simulation domain we extrapolate from measurements of the east-west ($E_x$) and north-south ($E_y$) components of the electric field in the F-region above Millstone Hill by making two assumptions. The first, that every (dipolar) field line is an equipotential, allows us to calculate the $\mathbf{E} \times \mathbf{B}$ drift everywhere on a field line once we know it anywhere on a field line. The second, that the (vertical) drift varies as $L^2$ at the magnetic equator, is valid when the electric field is curl-free and the azimuthal neutral wind dynamo is negligible [*Eccles*, 1998]. Given a drift at Millstone Hill of magnitude $v_M$ the magnitude of the drift at any other point in the simulation domain is

$$v_{E \times B} = v_M \sqrt{\frac{1 + 3\cos^2\theta_M}{1 + 3\cos^2\theta}} \left(\frac{\sin\theta}{\sin\theta_M}\right)^3 \left(\frac{L}{L_M}\right)^2, \tag{1}$$

where $\theta$ is the magnetic co-latitude. The direction of the drift is always perpendicular to $\mathbf{B}$ and hence varies along a field line.

The incoherent scatter radar at Millstone Hill measures three-dimensional ion velocities (from which the electric field can be determined) and meridional neutral winds with a time resolution of $\approx 30$ minutes. Typical errors are $\pm 0.2$ mV/m for the electric field and $\pm 20$ m/s for the wind. *Huang et al.* [2005] give a more complete description of the measurements. The two relevant components of the electric field as well as the corresponding $\mathbf{E} \times \mathbf{B}$ drifts are plotted in the top two panels of Figure 2. Because of the non-zero magnetic declination at Millstone Hill ($\approx -15°$) both the east-west and north-south components contribute to the drift, although the north-south contribution is minimal until $\approx 20$ UT on 3 April. At Millstone Hill a 3 mV/m east-west electric field implies a total drift speed of $\approx 60$ m/s and a vertically projected drift speed of $\approx 20$ m/s.

Unfortunately, although we have measurements of the average F-region meridional neutral wind above Millstone Hill, there is no straightforward way to extrapolate this data to the entire simulation domain. Moreover, we have no measurements of the zonal winds. We instead use the velocities (both meridional and zonal) from the empirical model HWM93. The model values for the meridional wind are plotted in the bottom panel of Figure 2 along with the observations. While the basic features of the data sets agree there are some notable differences, particularly in the magnitude of the wind during the early evening and pre-dawn hours (local time at Millstone Hill = UT-5). Possible effects of these discrepancies are discussed further in Section 4. Note that because of the large dip angle at Millstone Hill only 1/3 of the meridional wind speed is projected along the magnetic field.

SAMI2's empirical models of the neutrals and solar flux depend on the geophysical parameters $F_{10.7}$, $F_{10.7A}$ and Ap — the previous day's solar flux at 10.7 cm, the 81-day

centered average of $F_{10.7}$, and the Ap index. For both days $F_{10.7A} = 105.1$; on 2 April $F_{10.7} = 114.1$ and on 3 April $F_{10.7} = 108.6$. The daily Ap $= 3$ on 2 April and 41 on 3 April, but we also used finer gradations (e.g., 3-hour ap indices) in NRLMSISE-00 and HWM93.

## 3. Simulation Results

In Figure 3 we compare our simulation results to the observed electron densities and temperatures at an altitude of 330 km above Millstone Hill. The overall agreement is good, with the simulation successfully modeling the major changes between the quiet and active days. After the storm begins ($\approx 14$ UT on 3 April) the electron density quickly increases, peaking at $\approx 1.4 \times 10^6$ cm$^{-3}$, or roughly $2 - 3$ times the density at the same time on the previous day. Simultaneously the electron temperature drops by $\approx 1000$ K.

However several discrepancies can be seen. The first is in the electron temperature on 2 April when the model overshoots the observed value by roughly 10% at 12 UT and remains too high for several hours. This is probably due to the photoelectron heating model used in SAMI2 and is discussed further in Section 4. A second discrepancy is the $\sim 1$ hour lag between the onset of the simulated and actual storm on 3 April. Winds can cause such a delay by retarding the flow of material up a field line, but both the modeled and true meridional winds are relatively modest at this time. However HWM93 predicts a relatively large zonal wind ($\simeq 100$ m/s) during this period which, when projected onto the magnetic field, is large enough to cause the delay. An otherwise identical simulation that was performed with no zonal winds exhibited no lag in the storm onset.

To better show the effects of the storm on the F-region as a whole we plot $N_mF_2$ and $h_mF_2$ at Millstone Hill for both the observations and the simulation in Figure 4. $h_mF_2$ remained below 300 km during daylight hours on 2 April but during the storm on the following day it rose by $50 - 80$ km. Viewed from a fixed altitude of 330 km the rise of the F-region leads to an increase in the local electron density and a decrease in the electron temperature (see the top panel of Figure 3), i.e., cooler, denser plasma moves to higher altitudes. Note that this mechanism does not depend on what process lifts the F-region.

To test the relative importance of the electric field and the neutral atmosphere and winds in driving these large changes we performed two further simulations of the storm day. In the first we replaced the models of the neutral atmosphere and winds with their quiet day counterparts; in the second we used the storm day neutral atmosphere and winds and the quiet day electric field. The results are shown in Figure 5.

For the storm day electric field and the quiet day neutrals (dotted black line) the largest change from the original simulation is the $\sim 2$ hour delay in the ionosphere's response to the storm's onset. We attribute this to the neutral wind. The quiet day neutral wind is poleward which, as noted earlier, pushes plasma down the field line and suppresses, albeit not completely, the increase in electron density after 14 UT. There are also some minor differences in the temporal evolution of the electron density, particularly late in the storm $(20 - 22$ UT) when the simulation density rises as the observed density falls. In comparison the simulation with the quiet field and storm neutrals correctly captures the onset of the storm but diverges from the observations after 16 UT. In particular, this simulation underestimates the peak density by $\simeq 50\%$. We attribute this to the quiet

day electric field that changes from eastward to westward at $\simeq 18$ UT, thus pushing the F layer downward and reducing the electron density. Together these simulations suggest that the neutrals played a role in the initial stages of the storm but the electric field was the principal driver of the ionospheric evolution.

## 4. Discussion

We have presented a simulation study of storm-time effects on the mid-latitude ionosphere over Millstone Hill observatory using the NRL ionosphere code SAMI2. The simulation results agree reasonably well with the observations on both the quiet and the storm days. In particular, the model predicts the changes in the ionosphere over Millstone Hill relative to the previous (quiet) day: the F-peak altitude rose by $\approx 80$ km, the F-peak electron density increased by a factor of $\approx 2$, and the F-region electron temperature decreased by $\approx 1000$ K. We primarily attribute these dramatic changes to the long-lasting eastward electric field observed on the storm day between 12–20 UT that lifts cold, dense plasma to higher altitudes. We base this conclusion in large part on Figure 5, which indicates that the storm day neutral wind and quiet day electric field do not sufficiently account for the observations. By contrast, the active day electric field and quiet day neutral wind do capture the salient effects of the storm: a large enhancement in the electron density and decrease in the electron temperature.

The variations of the electron density and temperature with altitude were also measured around 19 UT on both the quiet and active days. Not surprisingly, in light of the data shown in Figure 4, *Huang et al.* [2005] found that the storm day had higher electron densi-

ties, lower electron temperatures, and higher $h_mF_2$s. Although the simulation agrees with these trends there are discrepancies, particularly in the temperature, at higher altitudes.

These differences may be due to SAMI2's treatment of photoelectron heating. Collisions are sufficiently frequent at low altitudes (below roughly 250 km, although there is some variation with the neutral density) that we assume photoelectrons deposit their energy locally. Above that point our model expresses the (non-local) heating as a function of the integral of the electron density along a field line. More sophisticated, but computationally intensive, approaches discretize the electron distribution function in energy space and solve some form of a Boltzmann transport equation. The transition between local and non-local heating is continuous in SAMI2, but during non-equilibrium periods unphysical short-lived temperature plateaus occasionally develop around 450 km. By making ad hoc adjustments to the details of our model we have established that these features have only minimal effects on the plasma at lower altitudes.

A thorough study of the origin of the prolonged, storm-time eastward electric field would require a coupled ionosphere-magnetosphere model that is beyond the scope of this Letter. However two possible sources are (1) a penetration electric field associated with a rapid change in the inner magnetospheric electric field at storm onset (e.g., *Kikuchi and Araki* [1979], *Foster and Rich* [1998]) and (2) a wind driven dynamo field associated with high-latitude heating of the atmosphere and the generation of equatorward neutral winds (e.g., *Fuller-Rowell et al.* [1994]). *Huang et al.* [2005] argued for a penetration electric field because it can quickly propagate to low latitudes, in agreement with the minimal lag between the storm onset and the ionospheric response seen in the data. Furthermore,

no strong equatorward winds were observed at Millstone Hill during the storm. (see the bottom panel of Figure 2).

A better comparison between simulations and data could be made with more realistic values for the neutral winds throughout the E and F regions. These can be obtained through either more detailed observations or a coupled thermosphere-ionosphere model. In the short term we will pursue the former approach using, for example, measurements taken at Millstone Hill for the September 2005 ISR World Month campaign (L. P. Goncharenko, private communication). Finally, we will also use SAMI3, an extension of SAMI2 to all longitudes, to investigate longitudinal effects such as the possible generation of inhomogeneous total electron content (TEC) enhancements by a poleward electric field (*Vlasov et al.* [2003]).

**References**

Bauske, R., and G. W. Prölls, Modeling the ionospheric response to traveling atmospheric disturbances, *J. Geophys. Res.*, *102*, 14,555, 1997.

Buonsanto, M. J., Ionospheric storms — a review, *Space Sci. Rev.*, *88*, 563, 1999.

Eccles, J. V., A simple model of low-latitude electric fields, *Geophys. Res. Lett.*, *103*, 26,699–26,708, 1998.

Foster, J. C., and F. J. Rich, Prompt midlatitude electric field effects during severe geo-
magnetic storms, *J. Geophys. Res.*, *103*, 26,367, 1998.

Fuller-Rowell, T. J., M. V. Codrescu, R. J. Moffett, and S. Quegan, Response of the
thermosphere and ionosphere to geomagnetic storms, *J. Geophys. Res.*, *99*, 3893, 1994.

Hedin, A. E., et al., Revised global model of the thermosphere winds using satellite and
ground-based observations, *J. Geophys. Res.*, *96*, 7657, 1991.

Huang, C.-S., J. C. Foster, L. P. Goncharenko, P. J. Erikson, W. Rideout, and A. J.
Coster, A strong positive phase of ionospheric storms observed by the Millstone
Hill incoherent scatter radar and global GPS network, *J. Geophys. Res.*, *110*, 2005,
doi:10.1029/2004JA010685.

Huba, J. D., G. Joyce, and J. A. Fedder, SAMI2 (Sami2 is Another Model of the Iono-
sphere): A new low-latitude ionosphere model, *J. Geophys. Res.*, *105*, 23,035–23,053,
2000.

Huba, J. D., K. F. Dymond, G. Joyce, S. A. Budzien, S. E. Thonnard, J. A. Fedder, and
R. P. McCoy, Comparison of $O^+$ density from ARGOS data analysis and SAMI2 model
results, *Geophys. Res. Lett.*, *29*, 2002, doi:10.1029/2001GL013089.

Huba, J. D., G. Joyce, and J. A. Fedder, Simulation study of mid-latitude iono-
sphere fluctuations observed at Millstone Hill, *Geophys. Res. Lett.*, *30*, 1943, 2003,
doi:10.1029/2003GL018018.

Jakowski, N., E. Putz, and P. Spalla, Ionospheric storm characteristics deduced from
satellite radio beacon observations at three European stations, *Ann. Geophys.*, *8*, 343,
1990.

Kikuchi, T., and T. Araki, Transient response of uniform ionosphere and preliminary reverse impulse of geomagnetic storm sudden commencement, *J. Atm. Terr. Phys.*, *41*, 917–925, 1979.

Lu, G., A. D. Richmond, R. G. Roble, and B. A. Emery, Coexistence of ionospheric positive and negative storm phases under northern winter conditions: A case study, *J. Geophys. Res.*, *106*, 24,493, 2001.

Picone, J. M., A. E. Hedin, D. P. Drob, and A. C. Aikin, NRLMSISE-00 empirical model of the atmosphere: Statistical comparisons and scientific issues, *J. Geophys. Res.*, *107*, 2002, doi:10.1029/2002JA009430.

Rishbeth, H., R. Gordon, D. Rees, and T. J. Fuller-Rowell, Modelling of thermospheric composition changes caused by a severe magnetic storm, *J. Atmos. Terr. Phys.*, *51*, 1283, 1985.

Vlasov, M., M. C. Kelley, and H. Kil, Analysis of ground-based and satellite observations of F-region behavior during the great magnetic storm of July 15,2000, *J. Atmos. Sol. Terr. Phys.*, *65*, 1223, 2003.
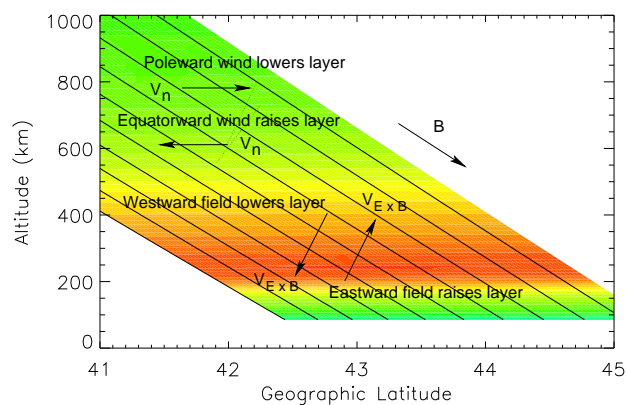
**Figure 1.**    Schematic of the effects of neutral winds and electric fields on the mid-

latitude ionosphere. The colors merely suggest the variation of the density with altitude
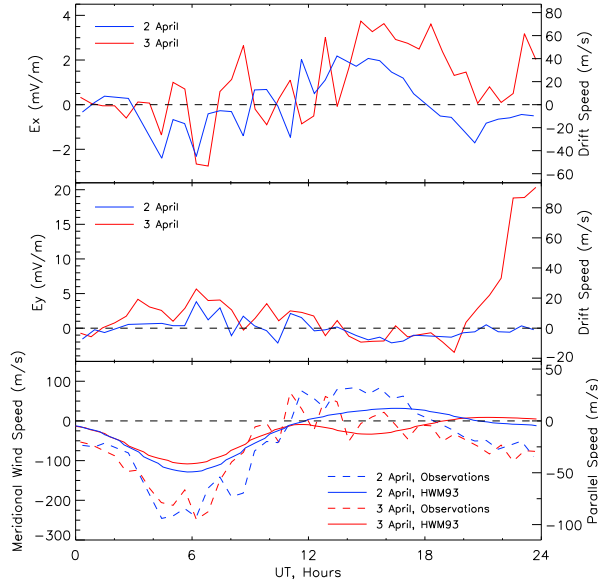
and do not represent the simulations.

**Figure 2.** F-region electric field components and neutral winds above Millstone Hill on 2 April (blue) and 3 April (red). For both the east-west ($E_x$, top panel) and north-south ($E_y$, middle panel) components the lines denote the observations and the simulations. The right axis gives the magnitude of the $\mathbf{E} \times \mathbf{B}$ drift at 330 km due to each component. In both panels upward and poleward drifts are positive. For the meridional neutral winds (bottom panel) the solid lines show the velocities from HWM93 and the dashed lines show the observations. The right axis gives the projection of the wind speed onto the local magnetic field. Positive values are northward.
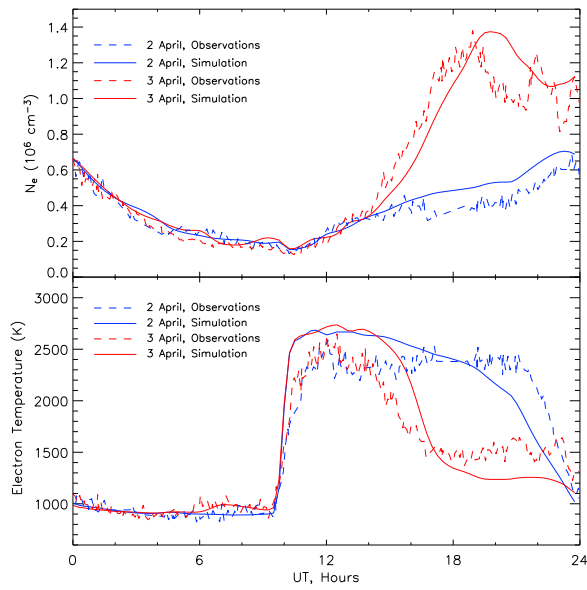
**Figure 3.** Comparison between observations (dashed lines) and simulation (solid) of the electron density (top) and temperature (bottom) at 330 km above Millstone Hill. Values from 2 April are shown in blue, 3 April in red.
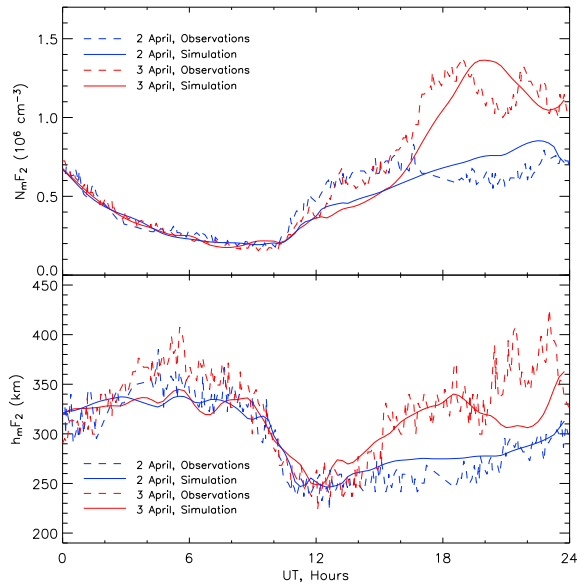
**Figure 4.** Comparison between observations (dashed lines) and simulation (solid) of $N_mF_2$ (top) and $h_mF_2$ (bottom) above Millstone Hill. Values from 2 April are shown in blue, 3 April in red.
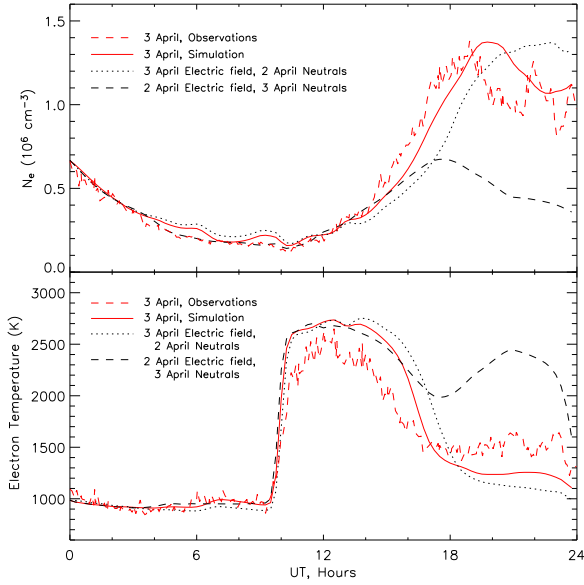
**Figure 5.** Electron density (top) and temperature (bottom) for simulations of 3 April. The observational data (dashed red) and normal simulation (solid red) are the same as in Figure 3. For the dashed black line the simulated electric field of 3 April has been replaced with that of 2 April. For the dotted black line the electric field is normal but the neutral atmosphere and winds have their 2 April values.